Triggering in a thermoacoustic system with stochastic noise

Iain C. Waugh[1,†,*] and Matthew P. Juniper[1]

[1]*Cambridge University Engineering Department, Trumpington Street, Cambridge, CB2 1PZ, United Kingdom*

[†]*Supported by EPSRC and IMechE funding*

[Submission: July 28, 2010; Revised Submission: February 01, 2011; Accepted: June 14, 2011]

ABSTRACT

This paper explores the mechanism of triggering in a simple thermoacoustic system, the Rijke tube. It is demonstrated that additive stochastic perturbations can cause triggering before the linear stability limit of a thermoacoustic system. When triggering from low noise amplitudes, the system is seen to evolve to self-sustained oscillations via an unstable periodic solution of the governing equations. Practical stability is introduced as a measure of the stability of a linearly stable state when finite perturbations are present. The concept of a stochastic stability map is used to demonstrate the change in practical stability limits for a system with a subcritical bifurcation, once stochastic terms are included. The practical stability limits are found to be strongly dependent on the strength of noise.

1. INTRODUCTION

In some linearly-stable thermoacoustic systems, self-sustained oscillations can be triggered by perturbations with amplitudes similar to the background noise level [1, Ch1 §IV]. This is known as triggering, or pulsed oscillation [2, 3]. An analogy has been suggested with bypass transition to turbulence in hydrodynamics [1, Ch1 §IV] [4]. Bypass transition to turbulence has been shown to rely not only on non-linearity, but also on non-normality [5]. Non-normality of the governing equations results in transient growth of small perturbations, even in regions where the system is linearly stable. This is a linear effect, but this transient growth can be large enough to excite the system into a region where non-linear effects become important. It has recently been shown that thermoacoustic systems are significantly non-normal [6, 7].

Analysis of bypass transition to turbulence with dynamical systems techniques has shown that one possible route to transition occurs via a complex network of saddle points and at least one local relative attractor [8]. The local relative attractor (an unstable attractor), has just one unstable eigenvalue so trajectories are attracted from the stable

[*]Corresponding Author: icw26@cam.ac.uk

directions but are then repelled in the one unstable direction. The exact trajectory depends sensitively on the initial location in state space. It has been shown that unstable attractors can exist for thermoacoustic systems [4], and it is suggested in this paper that, at the verge of triggering, the system evolves via the unstable attractors.

Emphasis in thermoacoustics has often been placed on the importance of linear stability, but in this paper we wish to emphasise the importance of practical stability. Linear analysis is valid for infinitesimal perturbations from the linearisation point, and linear stability implies that all infinitesimal perturbations will eventually decay. If the system has only one stable state, then linear stability further implies that all finite perturbations will eventually decay. If the system has more than one stable state, however, then linear stability can no longer imply that all finite perturbations will eventually decay. If a finite perturbation is large enough for the system to reach the basin of attraction of another stable state, then the original stable state is unstable to a perturbation of that size.

Practical stability is a measure of the stability of a state when finite perturbations are present [9], and has been studied in the context of chaotic attractors and shown to be important in their control [10, 11]. The difference between linear stability and practical stability is highlighted in figure 1. All three scenarios are linearly stable about the central point. When no other stable solutions exist, figure 1a, linear stability implies stability both to infinitesimal and finite perturbations. In figure 1b, three stable states exist and a large enough perturbation can excite the system to either of the other stable states. In figure 1c, the basin of attraction around the current stable state is much smaller and shallower, so a much smaller perturbation is required to reach either of the other stable states. Figure 1 b is thus more practically stable than figure 1c.

To define practical stability [9] we must first define what we consider to be 'stable', and then measure when this stability criterion is obeyed, in terms of the initial system condition, x_0, and perturbations in time $p(x, t)$. In the context of triggering, we will define stability here to be when the system remains in the basin of attraction of the steady state (fixed point at 0). The basin of attraction of the fixed point is termed Q, where $Q \subset \mathbb{R}^N$. We define the perturbations to be less than some magnitude: $\|p(x, t)\| \leq \delta$, $\delta \geq 0$, and we define the initial conditions to be bounded: $\forall x_0 \in Q_0 \subset Q$. If we have a dynamical system:

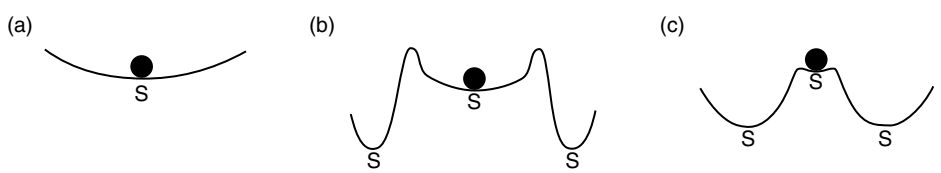

Figure 1: All three systems are linearly stable about the central point but, in (b) and (c), finite perturbations can excite the system to the other stable states. The system in (b) is more practically stable than in (c) because the central basin of attraction is larger and more attracting.

$$\frac{\partial x}{\partial t} = F(x,t) \tag{1}$$

With a permanently acting perturbation this becomes [9]:

$$\frac{\partial x}{\partial t} = F(x,t) + p(x,t) \tag{2}$$

Then the practical stability in a given time period is defined by Yang [9] to be:

"The solution x = 0 to Eq. (1) is said to be practically stable with respect to d, Q and Q_0 in finite time period [t_0, T], if for every perturbation p(x, t) with ||p(x, t)|| £ d the solution x(t_0, x_0, t) to Eq. (2) remains in Q for t Œ [t_0, T] and x_0 Œ Q_0."

This definition is complete, but it is difficult to compute basins of attraction for large nonlinear dynamical systems, and even more difficult to compute the action of the system under all possible perturbations $\|p(x, t)\| \leq \delta$. In this paper we aim to examine the practical stability of a thermoacoustic system under stochastic forcing, with perturbations, $p(t)$, that are independent of the current system state. Varying the mean amplitude of the perturbations will show how sensitive the practical stability is to background noise. The practical stability of the Rijke tube model to initial conditions has already been investigated by Juniper [12].

All physical thermoacoustic systems are subject to random noise, whether from incoming flow fields, combustion processes or mechanical vibration. Various types of noise have been shown to destabilise systems that are linearly stable when noiseless [2, 13–15] . Noise resulting from entropy and vorticity has also been shown to play a part in the process [2]. Non-normality has been highlighted as a key factor in the amplification of noise [16], and the susceptibility of a system to to be pushed out of the basin of attraction of the stable zero solution.

Stochastic delay differential equations have been studied, but mainly with linear analyses [14]. Ref. [14] showed that, for linear delay differential equations, additive noise has no effect on stability boundaries. Other studies examine the stochastic effects of parametric and multiplicative noise on a delay differential equation with a pitchfork bifurcation and show the resultant changes in stability boundaries [17]. Ref. [17] uses the result of [14] as evidence that additive noise will have no effect on stability boundaries. This paper aims to demonstrate that, in nonlinear systems, one of the key roles of noise is to force the system from one attracting state to another, not necessarily to change the stability boundaries.

When stochastic forcing is present, probability density functions (PDFs) have been used to describe the response of thermoacoustic systems in both experiments and theory [2, 15, 18–20]. These papers show that a single periodic solution creates a bimodal PDF, and that the addition of other stable solutions creates additional peaks. These did not, however, map these PDFs over a sub- or supercritical bifurcation as in other disciplines [17, 21].

The aim of this paper is to investigate the effect that noise has on triggering in a simple thermoacoustic system. The concept of a stochastic stability map is introduced in order to visualise the practical stability of a system under stochastic forcing. This can be used to define the region of practical stability of a thermoacoustic system for a given noise level.

2. GOVERNING EQUATIONS

The thermoacoustic system examined in this paper is identical to the simple Rijke tube model studied by Refs. [4, 6, 12], which contain a complete description. In summary, it is a tube of length L_0 in which a hot wire is placed $\tilde{x}_f$ from one end; §6.2 of [22]. A base flow is imposed through the tube with velocity u_0. The non-dimensional governing equations for momentum and energy are:

$$\frac{\partial u}{\partial t} + \frac{\partial p}{\partial x} = 0, \tag{3}$$

$$\frac{\partial p}{\partial t} + \frac{\partial u}{\partial x} + \zeta p - \beta\delta(x - x_f)\left(\left|\frac{1}{3} + u_f(t-\tau)\right|^{\frac{1}{2}} - \left(\frac{1}{3}\right)^{\frac{1}{2}}\right) = 0, \tag{4}$$

The system has four control parameters: ζ, which models the damping; β, which encapsulates all the information about the hot wire, base flow and ambient conditions; τ, which is the time delay between the velocity at the wire and the subsequent heat release and x_f, which is the position of the wire. The heat release term is based on the correlation by Heckl [23] and the heat release parameter, β, is equivalent to $k/\gamma M$ in [6]. The damping model is that used by Refs. [6, 24], and physically represents the energy lost by sound emitted from the ends of the tube and the energy lost to boundary layers at the tube walls [25].

For the system examined in this paper, $\partial u/\partial x$ and p are both set to zero at the ends of the tube. These boundary conditions are enforced by choosing an appropriate basis set:

$$u(x,t) = \sum_{j=1}^{N} \eta_j(t)\cos(j\pi x), \tag{5}$$

$$p(x,t) = -\sum_{j=1}^{N}\left(\frac{\dot{\eta}_j(t)}{j\pi}\right)\sin(j\pi x), \tag{6}$$

where the relationship between η_j and $\dot{\eta}_j$ has not yet been specified. In this Galerkin discretization, all the modes are orthogonal. It is important to point out that these modes are not, in general, the eigen-modes of the system. They are merely the basis set into which u and p are decomposed. The governing equations then reduce to two ordinary differential equations for each mode, labelled *j:*

$$\frac{\mathrm{d}}{\mathrm{d}t}\eta_j - j\pi\left(\frac{\dot{\eta}_j}{j\pi}\right) = 0, \tag{7}$$

$$\frac{\mathrm{d}}{\mathrm{d}t}\left(\frac{\eta_j}{j\pi}\right) + j\pi\eta_j + \zeta_j\left(\frac{\eta_j}{j\pi}\right) + 2\beta\sin(j\pi x_f)\times\left(\left|\frac{1}{3}+u_f(t-\tau)\right|^{\frac{1}{2}} - \left(\frac{1}{3}\right)^{\frac{1}{2}}\right) = 0, \tag{8}$$

where

$$u_f(t-\tau) = \sum_{k=1}^{N}\eta_k(t-\tau)\cos(k\pi x_f) \tag{9}$$

The state of the system is given by the amplitudes of the Galerkin modes that represent velocity, η_j, and those that represent pressure, $\dot{\eta}_j/j\pi$. These are given the notation $\mathbf{u} = (\eta_1,\ldots,\eta_N)^T$ and $\mathbf{p} \equiv (\dot{\eta}_1/\pi,\ldots,\dot{\eta}_N/N\pi)^T$. The state vector of the discretized system is the column vector $\mathbf{x} \equiv (\mathbf{u};\ \mathbf{p})$. The most convenient measure of the size of the perturbations is the acoustic energy per unit volume:

$$E = \frac{1}{2}u^2 + \frac{1}{2}p^2 = \frac{1}{2}\mathbf{x}^H\mathbf{x} = \frac{1}{2}\|\mathbf{x}\|^2, \tag{10}$$

where $\|\cdot\|$ represents the 2-norm.

Equations (7–8) can be linearized into the form $\mathrm{d}\mathbf{x}/\mathrm{d}t = \mathbf{L}\mathbf{x}$, from which it is found that $\mathbf{L}$ is non-normal [6]. (A non-normal operator satisfies $\mathbf{L}^H\mathbf{L} \neq \mathbf{L}\mathbf{L}^H$, where H denotes the Hermitian transpose.) Non-normality gives rise to linear transient growth, which is one of the main features of this paper.

3. DYNAMICAL SYSTEM BEHAVIOUR

The bifurcation diagram in figure 2 shows the periodic solutions of (7–8) with ($\zeta_j = 0.05\ j^2 + 0.01\sqrt{j}$, $x_f = 0.3$, $\tau = 0.02$ and $N = 20$, calculated with a numerical continuation tool for delay differential equations [26]. Figure 2 plots the minimum acoustic energy during the periodic solution as a function of β. The Floquet multipliers of all points on the periodic solutions are calculated to determine whether they are stable (solid lines) or unstable (dashed lines). Figure.2 is similar to those in Refs. [1, Ch1 Fig. 1.17] [27]. It is important to note that the lines in figure 2 are projections of the N-dimensional trajectories of the periodic solutions, and not fixed energy boundaries of the system.

Even though the system is linearly stable for $0 \le \beta \le 0.866$, it can support a low amplitude periodic solution for $\beta \ge 0.722$. The Hopf bifurcation at $\beta = 0.866$, $E = 0$, is where a pair of eigenvalues of the evolution operator have zero real part. This is the linear stability limit of the system. The Hopf bifurcation is sub-critical, resulting in an operating region $0.722 \le \beta \le 0.866$ where a low amplitude stable periodic solution and a stable zero solution are both possible. This is termed the bistable region here but has been referred to as the metastable region [15].

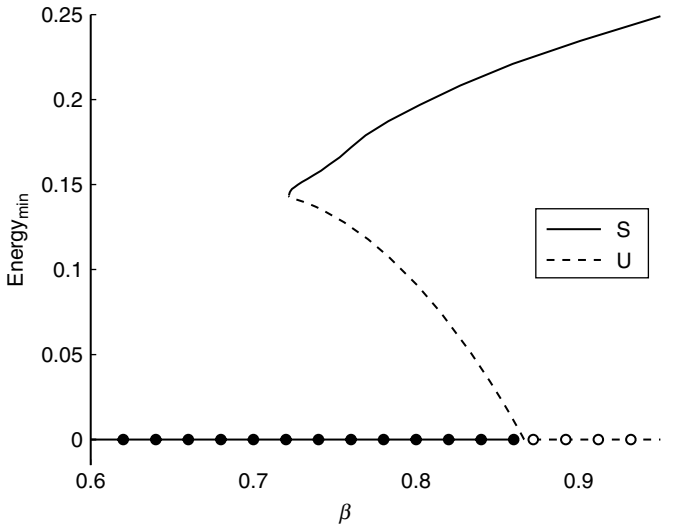

Figure 2: Bifurcation diagram for the 20-Galerkin mode system with $\tau = 0.02$. Dotted lines are steady states (fixed points), undotted lines are periodic solutions. A solid line represents a stable solution, and a dashed line represents an unstable solution.

The results in this paper are presented for N = 20, but have been calculated for N = 10, 20 and 50. The differences between the N = 20 and N = 50 results are negligible. The time-marching procedure used is similarly robust to changes in timestep.

From an initial state, the system converges to either a stable periodic solution or the zero solution. If the initial state is close to a stable solution, the system will be attracted towards it. If the initial state is far from a stable solution, however, the system can act more interestingly. Floquet analysis shows that the unstable periodic solution is unstable in one direction, marginally stable in another direction and stable in the remaining directions. The unstable periodic solutions attract trajectories during the transient phase, and then repel them along the unstable direction towards one of the stable solutions. Such manifolds are *unstable attractors,* and are found in physical systems such as pulse-coupled oscillators [28]. Their existence and behaviour in this Rijke tube model is demonstrated in Ref. [4]. In the triggering mechanism described in §4, the trajectories are first attracted towards the unstable periodic solution and then repelled to the stable periodic solution.

4. NOISE INDUCED TRIGGERING

The bifurcation diagram in figure 2 is shown for the noiseless system. In the bistable region, where both a stable zero solution and a stable periodic solution exist, the system can trigger from the former to the latter if perturbed strongly enough and this can occur via the unstable periodic solution. Refs. [4, 12] show that the basin of attraction of the

unstable periodic solution contains states with lower energy than the minimum energy on the periodic solution, due to non-normal and nonlinear growth around the unstable periodic solution. Therefore low amplitude noise may be enough to cause triggering via this mechanism.

In this section, we consider triggering to the stable periodic solution in figure 2. The practical stability of the system will be examined when stochastic noise is present. Low levels of noise will be seen to initiate triggering and cause the system to be practically unstable in some operating conditions. Multiple random noise signals will be used to examine the practical stability of the system in a probabilistic manner.

4.1. Noise definition

Noise can be divided conceptually into four types: additive noise, where a small forcing is added continually to the system; parametric noise, where coefficients in the governing equations vary; multiplicative noise, where noise amplitude is proportional to the current state of the system [15]; and modal noise, where energy is redistributed between the Galerkin modes without any overall change in energy.

Noise is added to the heat release term in equation (8) to give equation (11), where u_N is the noise term. This simple noise model examines the response of the heat release to base flow noise at the wire. (General base flow noise propagating through the tube would require the tube boundary conditions to be relaxed, which is beyond the focus of this study.) The noise profile is independent of the current state of the system when added to u_f, but the action of the noise is not purely additive or independent of the system state because it must combine with u_f within the modulus and square root. It is a mixture of multiplicative and additive noise. A purely additive noise signal will be analysed in section 4.4 and shown to produce similar results.

$$\frac{\mathrm{d}}{\mathrm{d}t}\left(\frac{\dot{\eta}_j}{j\pi}\right)+j\pi\eta_j+\zeta_j\left(\frac{\dot{\eta}_j}{j\pi}\right)+2\beta\sin(j\pi x_f)\times\left(\left|\frac{1}{3}+u_f(t-\tau)+u_N(t-\tau)\right|^{\frac{1}{2}}-\left(\frac{1}{3}\right)^{\frac{1}{2}}\right)=0, \quad (11)$$

The noise signal is generated by defining an amplitude distribution in the frequency domain and assigning random phases to each discretised frequency. An inverse Fourier transform is applied to the noise frequencies to form the noise signal in the time domain. This method allows us to control the noise spectrum, and results in a signal that is random and non-periodic over the time domain. We have found that results for this simple noise model are qualitatively similar to those using noise generated by the rigorously stochastic Ornstein-Uhlenbeck process [29].

The Rijke tube model used in this paper has previously been shown to respond more strongly to low frequency noise [4]. Noise that has higher amplitudes at low frequencies, herein referred to as pink noise, will be used for the remainder of this paper. A sample pink noise spectrum and time domain trace are shown in figure 3. The spectrum is chosen to be a smooth function that is rich in lower frequencies. Higher frequency noise, which has lower correlation time, also induces triggering but requires a higher noise strength.

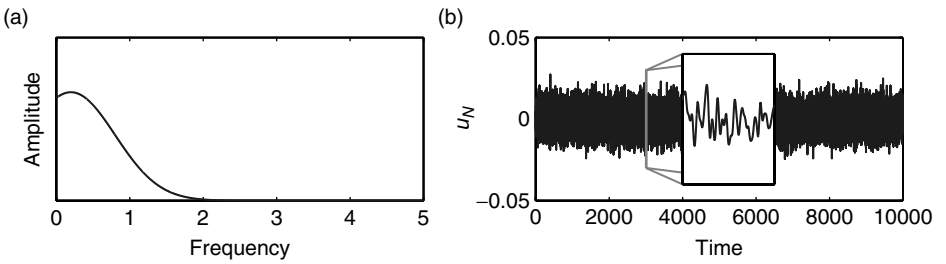

Figure 3: Pink noise profile in (a) the frequency domain and (b) the time domain, with a strength of 0.5%. The enlarged portion of the trace in (b) is 20 time units long.

The noise profile is not periodic so the maximum amplitude is not a good measure of the noise strength. The noise strength in this paper is quantified by the averaged absolute value of the noise signal, u_N, normalised by u_0. A root mean square measure could also have been used.

4.2. Triggering mechanism

When sufficient noise is added, the model triggers to self-sustained oscillations as expected. If the strength of a particular noise signal is increased to the point where it first triggers then the system evolves via the unstable periodic solution. This is shown in figure 4a and 4b, where a fractional increase in noise strength results in triggering. If the noise strength is increased further then the system evolves directly to the stable periodic solution. This is shown in figure 4c and in Ref. [4].

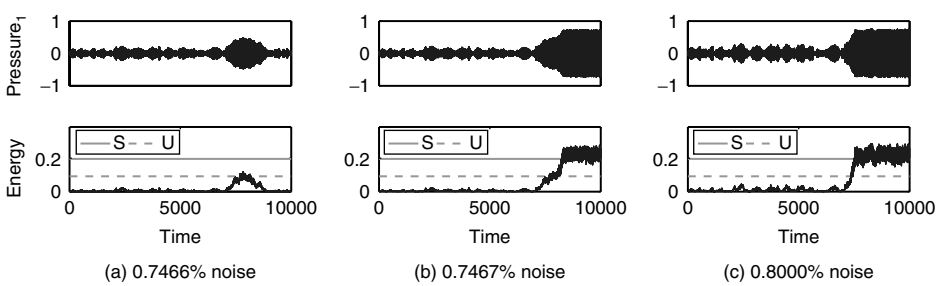

Figure 4: The system behaviour with $\beta = 0.8$ for a noise profile with amplitudes of (a) 0.7466%, (b) 0.7467%, (c) 0.8000%. The role of the unstable periodic solution in the triggering process is evident in (a) and (b), where a small increase in noise results in triggering. With the higher noise amplitude in (c), however, the system triggers directly to the stable periodic solution. Pressure traces in this paper are shown for the fundamental mode only, which contains most of the perturbation energy.

At the limit of triggering, the trajectory of the system is affected by the proximity of the unstable periodic solution to the stable zero solution. In figure 6 we plot the system response to noise at the limit of triggering for the three values of β identified in figure 5. In figure 6c, only weak noise is required to reach the unstable periodic solution and the system stays near the unstable periodic solution for many cycles. In figure 6b, stronger noise is required to reach the unstable periodic solution and the system stays near the unstable periodic solution for few cycles.

A conceptually different response is shown in figure 6a, where the energy of the unstable periodic solution is close to that of the stable periodic solution. (Energy alone is not enough to quantify the proximity of two trajectories in N-dimensional state space, but both trajectories are rich in the lower Galerkin modes and are close in state space.) The strong noise in this simulation quickly triggers the system to the stable periodic

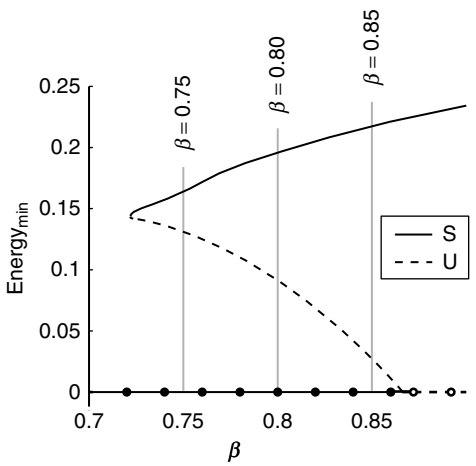

Figure 5: Bifurcation diagram showing β values considered in figure 6.

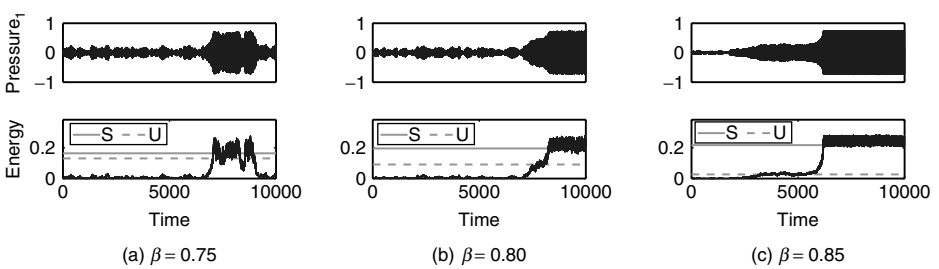

Figure 6: Triggering at three different values of β, as illustrated by figure 5. Noise is applied with strength (a) 1.2%, (b) 0.73% and (c) 0.25%.

solution and is also strong enough to dislodge the system back to the zero solution. The ability of the noise to link the basin of attractions of the stable solution and zero solution is examined further in §4.3.

The pressure trace of figure 4b is similar to that seen in the experiments of Ref. [19, fig. 15b], in which the oscillations "first jump up rapidly, then stay relatively constant, and then smoothly increase". These experiments could indicate the presence of an unstable attractor in a real combustor.

The region of practical instability for a particular noise strength can be visualised by examining the trends of repeated runs. Here 4000 evolutions of 10000 time steps are calculated for each value of β and noise strength, and the trends are plotted in figure 7. The percentage of runs that results in triggering is shown in figure 7a for three different noise levels. For each noise level, there is a sharp transition between the β values that do and do not result in triggering. The points are fitted with functions of the form $y = 50$ erf $(a\,(x - \mu)) + 50$, where a and μ are scaling and shifting constants. As noise strength increases, this transition occurs at lower values of β, further away from the Hopf bifurcation. This shows qualitatively the same result as Ref. [21, Fig. 10], where the most probable amplitudes and average amplitudes are plotted for an electronic oscillator with increasing noise. Above the linear stability limit ($\beta > 0.866$), all runs reach the periodic solution. This is due to linear amplification of perturbations followed by nonlinear saturation to the periodic solution, rather than triggering.

It is also important to understand whether triggering is immediate or delayed. The trend of average time to triggering is plotted in figure 7b. We define triggering to have occured after the system has spent several cycles at the amplitude of the periodic solution. For each noise level, the average time to triggering decreases as the system nears and enters the linearly unstable region. An increase in noise strength results in a drop in average time to triggering at each β location. Above the linear stability limit

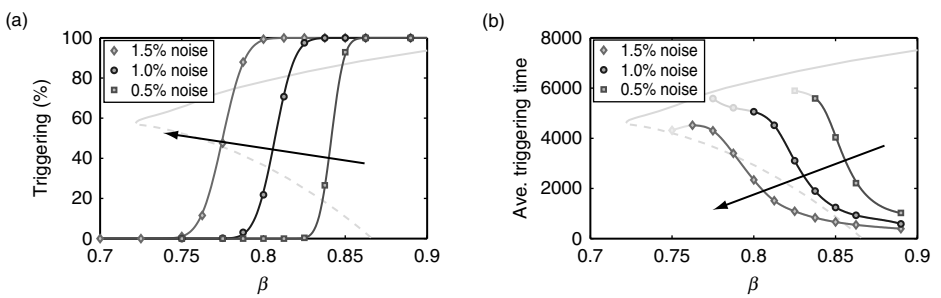

Figure 7: Results from 4000 runs of 10000 time units with randomly generated pink noise. The plots show (a) the percentage of triggering incidences and (b) the average time to triggering, for noise of strengths 1.5%, 1% and 0.5%. Fainter points in (b) have larger errors due to their low triggering rate. Arrows show the direction of increasing noise.

($\beta > 0.866$), a finite time is still required for the system to linearly amplify the pertubations and saturate to the periodic solution.

4.3. Stochastic stability maps

As demonstrated in §4.2, a system with a subcritical bifurcation can be triggered with low amplitude noise. In the presence of noise, therefore, the linear stability limit in a bistable region can be misleading. To analyse the practical stability of the system with stochastic noise, a probabilistic approach must be used. The concept of a stochastic stability map is introduced in this section.

Figure 7 shows how likely a system is to trigger as a function of noise and β but gives no other information. For a given energy-time trace, such as figure 8, the time spent by the system at each energy level can be quantified by dividing the energy signal into quantisation levels and calculating a probability density function (PDF). In this figure, the increase in the PDF around energy of 0.2–0.3 shows that the system has triggered.

If enough time series of a set length are examined for a particular β and noise strength, but with randomly generated noise signals, then a smooth average PDF is created. The PDF depends on the length of the time window, particularly for time windows that are of the same order as the average triggering time. This sensitivity is particularly evident around the linear stability limit, where triggering is very likely to occur for a given noise level. If enough time series of a long enough length are used, however, then the PDFs become a useful quantity to define a stable operating region.

For a fixed noise level, this process can be repeated at different β values and the 2D slices combined to form a surface. We refer to this as a stochastic stability map, shown in figure 9 for 6 levels of increasing noise, where the greyscale represents the PDF. The bifurcation diagram of mean oscillation energy and the linear stability limit (vertical line) are superimposed onto each map.

In the absence of noise, the system would only reach self-sustained oscillations beyond the linear stability limit. In figure 9a only a small amount of noise is applied.

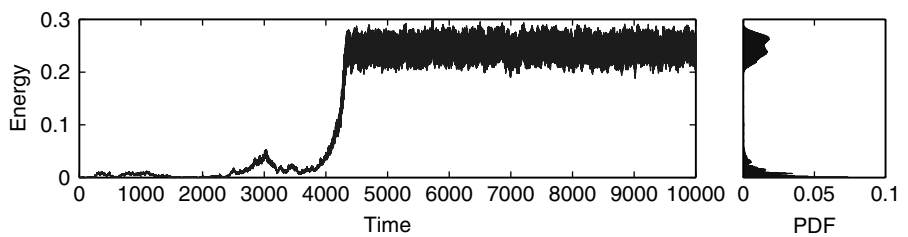

Figure 8: An energy-time trace is taken for $\beta = 0.85$, with noise of 0.5%. The energy of the system is divided into quantisation levels, and a normalised PDF created from the energy-trace. PDFs from multiple time traces can be averaged for a set noise strength and β, to obtain a smoother curve which is then used as a 2D slice in figure 9.

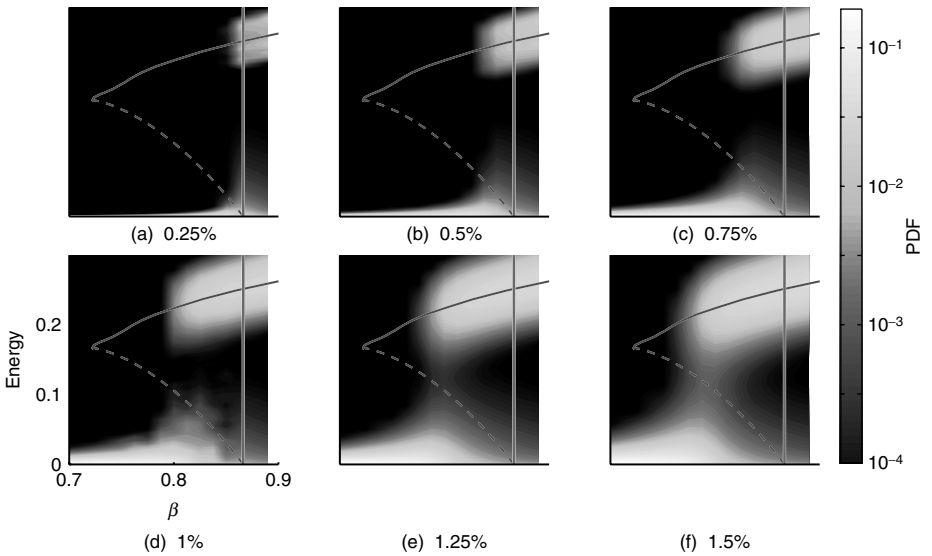

Figure 9: Probability Density Functions (PDFs) of the system energy with increasing velocity noise strength, against the bifurcation diagram of the noiseless system. The bifurcation diagram for the noiseless system is plotted for the mean energy of the periodic solutions. The PDFs are generated with 4000 runs of 10000 time units for each β and noise strength combination. The vertical line marks the onset of linear instability. A floor of 10^{-4} is applied to the PDF data for plotting.

The stochsatic stability map shows that the system will reach self-sustained oscillations beyond the linear stability limit, but also shows the system is likely to trigger slightly before it. As the strength of noise is increased in figure 9b–c, this region of triggering extends to lower values of β. There is a sharp transition between β values that do and do not trigger, which is also seen in figure 7. The system starts from rest so, even beyond the linear stability limit, some time is required for the system to reach the stable periodic solution. Consequently, the PDF value near the zero solution in figure 9 and the average time to triggering in figure 7b are non-zero.

Figure 9b–c correspond to the cases in figure 6b and c, where the noise level is just high enough to cause triggering, but not large enough to dislodge the system back to the zero solution. This is seen in the PDF diagrams, in which the system lies in two distinct regions. One is between the zero solution and the unstable periodic solution, the other is around the stable periodic solution. This shows that, once the unstable periodic solution is reached, the system quickly reaches the stable periodic solution and is unlikely to return. The PDFs in this region are qualitatively the same the theoretical results from the combustion chamber model of [2].

In figure 9d–f a bridge develops between these two regions around $\beta = 0.8$. This bridge corresponds to energy traces such as in figure 6a. Here the noise is strong enough to trigger the system from the zero solution to the stable periodic solution and also strong enough to dislodge the system back from the stable periodic solution to the zero solution. This forms bursts of high energy oscillations as seen in figure 6a. At the same noise level, the bridge is much less pronounced at higher β, because the unstable periodic solution is further from the stable periodic solution, and therefore the system is less easily dislodged from the stable periodic solution.

The formation of the bridge can be seen clearly in figure 10. This plots 2D slices through the stochastic stability maps at three locations on the bifurcation diagram, as shown in figure 5. The PDFs of four different noise levels are compared at these three locations. When the energy of the unstable periodic solution is high, as in figure 10a, none of the noise strengths result in triggering. As the noise increases, the spread around the zero solution increases. In figure 10b, this spread comes close enough to the unstable periodic solution that the system can trigger to the stable periodic solution. In figure 10c, as the noise increases, the probability of triggering and the spread around both stable solutions increase.

These results are qualitatively the same as those of Ref. [30], who studied a non-normal model of magnetic energy in a turbulent dynamo, which exhibits a subcritical bifurcation. By including multiplicative noise in the model, their system triggers from the zero fixed point to the basin of attraction of a second fixed point. This lowers the PDF around the zero fixed point and creates a new peak around the second fixed point. If their noise intensity is increased further, their system can be dislodged back into the

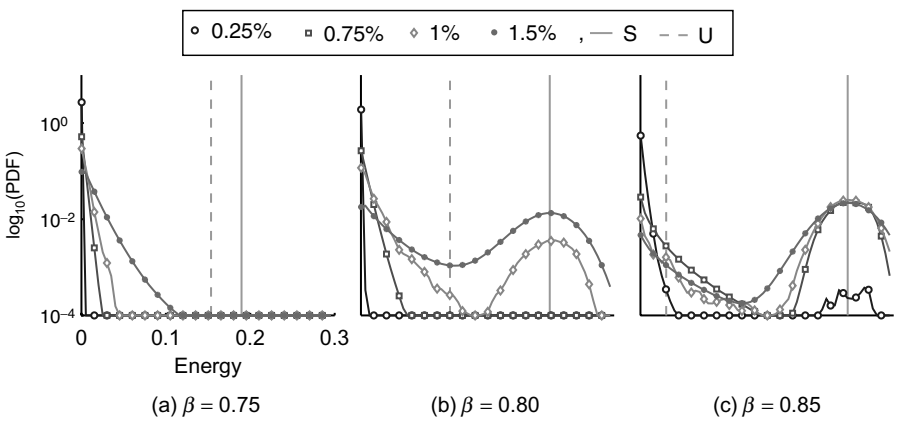

Figure 10: Probability Density Functions (PDFs) of the system energy at three values of β, as shown in figure 5, with increasing noise. The results are plotted for 4000 runs of 10000 time units for each β and noise combination. A floor of 10^{-4} is applied to the PDF data.

basin of attraction of the zero fixed point. The same process can also dislodge their system into the basin of attraction of a third fixed point.

System responses such as in figure 6a, where the system displays quiet periods between periods with self-sustained oscillations, were also predicted using multiplicative noise in the model of [15, Fig. 5b]. It was assumed that this was due to the hysteresis region of a subcritical bifurcation. This may be true in the case of multiplicative noise, which moves the stability boundaries of the system, but is qualitatively different from the mechanism seen in this paper. Here the bimodal PDF results from noise dislodging the system from the stable solution to the zero solution.

Ref. [16] neatly highlights the importance of non-normality in triggering by considering a model of transition to turbulence. The probability of leaving the basin of attraction of the zero solution is plotted against a non-normality parameter for different strengths of noise [16, Fig. 1]. This probability increases with the noise strength, and increases strongly with the degree of non-normality. In combustors, the degree of non-normality and transient growth is large [7]. The Rijke tube model exhibits transient energy growth with a factor of around 1.4, whereas more complex thermoacoustic models have factors of around 10^6 [7]. This will result in a stronger magnification of background noise and triggering with lower noise strengths.

4.4. Additive noise

It has been shown with linear analyses that pure additive noise does not change stability boundaries [14]. In a nonlinear system, however, there may be multiple stable states. Additive noise does not change the stability boundaries of the system, but it may excite the system into the basin of attraction of another stable state. This section aims to show that purely additive noise will affect the practical stability of the system in a similar way to the velocity noise used in section 4. A purely additive noise signal is defined, $\varepsilon(t)$, with the same low frequency spectrum as $u_N(t)$ in section 4.1, and it is added to the governing equations (12). The strength of the noise is quantified by the averaged absolute value of the noise trace, normalised by one half of the pressure non-dimensionalisation quantity, $\rho_0 \gamma M$

$$\frac{\mathrm{d}}{\mathrm{d}t}\left(\frac{\eta_j}{j\pi}\right) + j\pi\eta_j + \zeta_j\left(\frac{\eta_j}{j\pi}\right) + 2\beta\sin(j\pi x_f)\times\left(\left|\frac{1}{3}+u_f(t-\tau)\right|^{\frac{1}{2}} - \left(\frac{1}{3}\right)^{\frac{1}{2}}\right) = \varepsilon_{jN}(t), \qquad (12)$$

The stochastic stability map for the system under additive noise is shown in figure 11. The trends are qualitatively similar to those obtained for the velocity noise. The stochastic stability map shows that the system will reach self-sustained oscillations beyond the linear stability limit, but also shows the system is likely to trigger slightly before it. As the strength of noise is increased in figure 11b–c, this region of triggering extends to lower values of β. In figure 11d–f, a bridge again develops between the two stable.

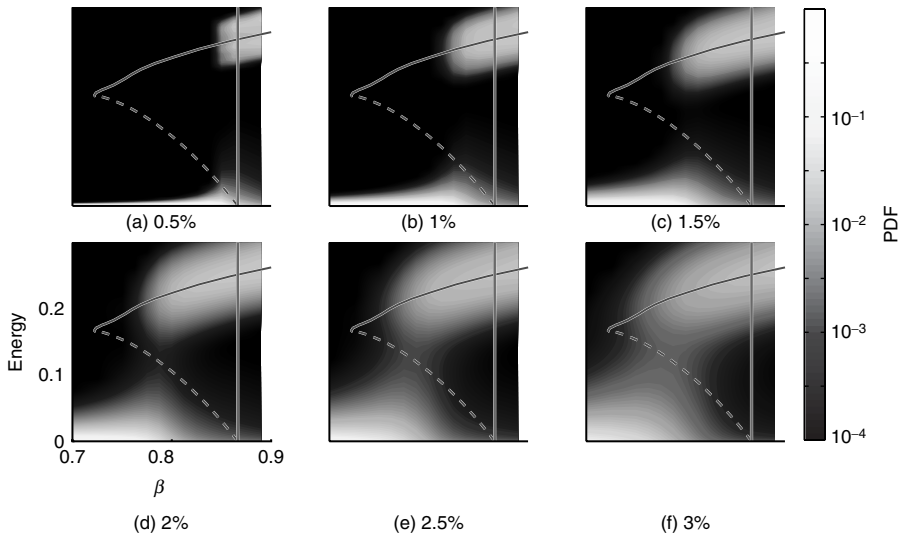

Figure 11: Probability Density Functions (PDFs) of system energy with increasing additive noise strength, against the bifurcation diagram of the noiseless system. The bifurcation diagram for the noiseless system is plotted for the mean energy of the periodic solutions. The PDFs are generated with 4000 runs of 10000 time units for each β and noise strength combination. The vertical line marks the onset of linear instability. A floor of 10^{-4} is applied to the PDF data for plotting.

5. CONCLUSIONS

This paper explores the triggering mechanism in thermoacoustics, and the role of stochastic noise in the process. The behaviour of a simple thermoacoustic system [4, 6, 12] is examined under stochastic forcing. It is shown that this system evolves via the unstable attractor at the limit of triggering.

Triggering strongly depends on the strength of the noise and the parameter β. The system is shown to be practically unstable below the linear stability limit in the presence of low strength noise. As noise strength increases, the system becomes practically unstable further from the Hopf point, increasing the region where triggering may occur. As noise strength increases further the system can be dislodged from the stable periodic solution to the zero solution. This results in quiet periods and intermittent bursts of high energy oscillations.

Stochastic stability maps are introduced in order to visualise the practical stability of a thermoacoustic system under stochastic perturbations. Stochastic stability maps quantify the probability that the system lies within a particular state. These show that the PDFs are bimodal in the operating regions that can trigger. The amplitude of the stable periodic solution with noise agrees well with that predicted by the noiseless bifurcation diagram. If the level of noise in a real combustion system is known, then a stochastic

stability map could be used to predict the region of safe operation. Alternatively, multiple experimental results could be compile into a stochastic stability map in order to visualise the practical stability of the system under operating conditions.

Non-normal transient growth is influential in the magnification of small perturbations in a thermoacoustic system, and therefore in triggering due to noise. Even though the thermoacoustic system examined in this paper is only slightly non-normal, it exhibits significant transient growth towards an unstable attractor. Transient growth is likely to be even more important in complex thermoacoustic models, which are significantly more non-normal [7].

REFERENCES

[1] T.C. Lieuwen and V. Yang. *Combustion instabilities in gas turbine engines.* AIAA, 2005.

[2] V.S. Burnley and F.E.C. Culick. Influence of Random Excitations on Acoustic Instabilities in Combustion Chambers. *AIAA Journal*, 2000, 38(8).

[3] N. Ananthkrishnan, S. Deo, and F.E.C. Culick. Reduced-order modeling and dynamics of nonlinear acoustic waves in a combustion chamber. *Combustion Science and Technology,* 2005,177: 221–247.

[4] I. Waugh, M. Geuβ, and M. Juniper. Triggering , bypass transition and the effect of noise on a linearly stable thermoacoustic system. *Proceedings of the Combustion Institute*, 2010, 33.

[5] P. Schmid and D.S. Henningson. *Stability and transition in shear flows.* Springer, 2001.

[6] K. Balasubramanian and R.I. Sujith. Thermoacoustic instability in a Rijke tube: Non-normality and nonlinearity. *Physics of Fluids*, 2008, 20: 044103.

[7] K. Balasubramanian and R.I. Sujith. Non-normality and nonlinearity in combustion-acoustic interaction in diffusion flames. *Journal of Fluid Mechanics,* 2008, 594: 29–57.

[8] Y. Duguet, A.P. Willis, and R.R. Kerswell. Transition in pipe flow: the saddle structure on the boundary of turbulence. *Journal of Fluid Mechanics,* 2008, 613: 255–274.

[9] X. Yang. Practical stability in dynamical systems. *Chaos, Solitons & Fractals*, 2000, 11:1087–1092.

[10] T. Kapitaniak and J. Brindley. Practical Stability of Chaotic Attractors. *Chaos, Solitons & Fractals,* 1998, 9(1): 43–50.

[11] T. Kapitaniak and J. Brindley. Practical Stability of Synchronized Chaotic Attractors and its Control. *Proceedings of the 7th Mediterranean Conference on Control and Automation*, 1999, pages 1224–1230.

[12] M. Juniper. Triggering in the horizontal Rijke tube: non-normality, transient growth and bypass transition. *Journal of Fluid Mechanics*, 2010, 667: 272–308.

[13] T. Lieuwen and A. Banaszuk. Background noise effects on combustor stability. *Journal of Propulsion and Power*, 2005, 21(1): 25–31.

[14] M.C. Mackey and I.G. Nechaeva. Solution moment stability in stochastic differential delay equations. *Physical Review E,* 1995, 52(4): 3366–3376.

[15] P. Clavin, J.S. Kim, and F.A. Williams. Turbulence-Induced Noise Effects on High-Frequency Combustion Instabilities. *Combustion Science and Technology*, 1994,96(l): 61–84.

[16] S. Fedotov, I. Bashkirtseva, and L. Ryashko. Stochastic analysis of a non-normal dynamical system mimicking a laminar-to-turbulent subcritical transition. *Physical Review E,* 2002, 66(6): l–6.

[17] M. Gaudreault, F. Lépine, and J. Viñals. Pitchfork and Hopf bifurcation thresholds in stochastic equations with delayed feedback. *Physical Review E*, 2009, 80(6): l–8.

[18] T. Lieuwen. Statistical characteristics of pressure oscillations in a premixed combustor. *Journal of Sound and Vibration*, 2003, 260(1): 3–17.

[19] T. Lieuwen. Experimental Investigation of Limit-Cycle Oscillations in an Unstable Gas Turbine Combustor. *Journal of Propulsion and Power*, 2002, 18(l): 61–67.

[20] F. E. C. Culick, M. V. Heitor, and J. H. Whitelaw. *Unsteady Combustion.* Springer, 1996.

[21] R. Berthet, A. Petrossian, S. Residori, B. Roman, and S. Fauve. Effect of multiplicative noise on parametric instabilities. *Physica D: Nonlinear Phenomena,* 2003, 174(l–4): 84–99.

[22] A. Dowling and J.E. Ffowcs-Williams. *Sound and sources of sound.* Ellis Horwood, 1983.

[23] M.A. Heckl. Non-linear acoustic effects in the Rijke tube. *Acustica*, 1990, 72: 6371.

[24] K. Matveev. Thermoacoustic Instabilities in the Rijke Tube: Experiments and Modeling. *PhD. Thesis, California Institute of Technology*, 2003.

[25] L. D. Landau and E. M. Lifshitz. *Fluid Mechanics.* Pergamon Press, 1959.

[26] K. Engelborghs, T. Luzyanina, and D. Roose. Numerical bifurcation analysis of delay differential equations using DDE-BIFTOOL. *ACM Transactions on Mathematical Software*, March 2002, 28(1): 1–21.

[27] N. Noiray, D. Durox, T. Schuller, and S. Candel. A unified framework for nonlinear combustion instability analysis based on the flame describing function. *Journal of Fluid Mechanics,* 2008, 615: 139–167.

[28] P. Ashwin and M. Timme. Unstable attractors: existence and robustness in networks of oscillators with delayed pulse coupling. *Nonlinearity,* 2005, 18(5): 2035–2060.

[29] W. Horsthemke and R. Lefever. *Noise-induced transitions.* Springer-Verlag Berlin, 2006.

[30] S. Fedotov, I. Bashkirtseva, and L. Ryashko. Stochastic analysis of subcritical amplification of magnetic energy in a turbulent dynamo. *Physica A: Statistical Mechanics and its Applications*, 2004, 342(3–4): 491–506.